Detection of Regular Rotational Activity During Cardiac Arrhythmia Using the Helmholtz Decomposition for Directed Graphs

Sebastiaan Lootens[1], Vineesh Kappardan[2], Balvinder Handa[2], Fu Siong Ng[2], Nele Vandersickel[1]

[1]Department of Physics and Astronomy, Ghent University, Ghent, Belgium
[2]Imperial College London, London, United Kingdom

Abstract

This paper introduces a novel method to detect re-entry called DGM-CURL based on the Helmholtz Decomposition for directed graphs, fully integrated into our open-source software OpenDGM. We apply this method alongside two existing methods Phase Mapping (PM) and Directed Cycle Search (DGM-CYCLE) to assess their degree of agreement. Four datasets are explored: (1) simulated two-dimensional functional re-entry, (2) simulated three-dimensional anatomical re-entry, (3) clinical electroanatomical atrial tachycardia (AT) mapping data (4) experimental rat ventricular fibrillation (VF) data. Results indicate general agreement between all three methods. Applying the Helmholtz decomposition to edge weights equal to the differences in local activation time, we observe that large values indicate graph nodes conserving the in- and output of these differences in the original graph, highlighting areas of re-entry. We stress the importance of using multiple algorithms to detect rotational activity as each method is prone to errors. Using a combined approach decreases this susceptibility to errors and offers a more complete picture of the dynamics of rotational drivers in cardiac arrhythmia.

1. Introduction

Cardiac arrhythmia are characterized by an abnormal heart rhythm resulting from the obstruction of the normal conduction of electrical wave propagation in the heart. Rotational electrical activity or re-entry is widely accepted as one of the main mechanisms sustaining this disease [1]. There are two types of re-entry: anatomical, where waves circle structures like pulmonary veins or scar tissue, and functional, where waves rotate around their refractory tail. Thus, re-entry localization is crucial to guide ablation strategies, which aim to burn the cardiac tissue to eliminate this rotational activity by introducing conduction blocks.

Recently, a novel open-source software package OpenDGM was developed to analyze rotational activity in electroanatomical mapping data ranging from simulated, experimental, and clinical data [2]. DGM creates a directed graph using a conduction velocity threshold from a set of points in space containing local activation time (LAT) values. Afterward, directed cycles can be identified using standard graph theory algorithms, which have been shown to correlate to rotational centers sustaining cardiac arrhythmia such as atrial tachycardia (AT). However, cycle search has disadvantages, such as its inability to detect incomplete rotations, also crucial as driver of the AT [3].

Therefore, we present DGM-CURL, a novel method for the detection of anatomical and functional re-entry. This method used the Helmholtz decomposition for directed graphs, retrieving the curl component of the graph. This component has the property that ingoing edge weights equal outgoing edge weights, which is satisfied for areas corresponding with re-entry. As such, this method holds the potential for identifying and localizing re-entrant circuits. Thus, this work aims to compare DGM-CURL to existing methods such as Phase Mapping (PM) and cycle search (DGM-CYCLE) for the detection of functional and anatomical re-entry in simulated, experimental, and clinical data.

2. Datasets

(1) A **two-dimensional rotor simulation** without fibrosis was conducted using the LuoRudy91 [4] model in OpenCARP [5] with GCa = 0, GNa = 22, and GK = 0.423 mS/cm². A 100.1 x 100.1 mm² mesh with 0.3112 S/m conductivity resulted in a 0.77 mm/ms conduction velocity. The S1S2 protocol initiated the rotor. Details can be found in Lootens et al. [6]. (2) **Simulated Atrial Tachycardia (AT)** was performed in OpenCARP on a 40 mm spherical mesh using the ten Tusscher-Panfilov [7] model. L-type calcium current ICaL was reduced by 70%, and rapid delayed rectifier potassium current IKr increased by 70%. AT was induced using S1-S1 pacing at 250 ms along a path 4 mm from a block line. (3) A **clinical human AT** case from Städische Klinikum in Karlsruhe with three boundaries was used. Criteria included sufficient electroanatom-

ical map quality (≥ 0.005 points/mm²), confirmed diagnosis, known boundary locations, and TCL before/after ablation. LATs were preprocessed using a peak-to-peak threshold of 95% on the LAT gradient and DBSCAN clustering on the LAT values. (4) **Experimental VF data** was analyzed in Chapter 5 of Handa et al. [8], involving ex vivo rat hearts using the Langendorff apparatus. VF was induced and recorded using optical mapping. Signal processing included 3×3 binning, a 50th-order FIR filter, and zero-phase filtering. For details, see Laughner et al.[9].

3. Methods

3.1. Phasemapping (PM)

The phase mapping procedure involves three steps. First, phase maps are constructed: using the method from Roney et al. [10] for simulated rotors, the Sawtooth Method for AT simulations and clinical data, and the method from Siong et al. [9] for experimental rat VF data. Second, neighbor rings are formed according to Rantner et al. [11]. The points are sampled using a distance threshold $\mathbf{r_s}$, and a Voronoi mesh is created. Each mesh node calculates its n-th nearest neighbors up to $n_{\max}$, stored as a sparse matrix for efficiency. These neighbors are sorted by projecting to the best-fitting plane using Singular Value Decomposition. Third, Phase Singularity (PS) points are tagged which are points where the topological charge n_t calculated from the difference between the number of positive/negative phase jumps $n(\text{PJ}_\pm)$ (above/below $\pm\pi$) is non-zero, as seen in equation (1). This PS detection excludes loops with undefined phase (NaN values) like scar tissue.

$$n_t = n(\text{PJ}_+) - n(\text{PJ}_-) \tag{1}$$

3.2. Directed graph building (DGM-CYCLE and DGM-CURL)

A prerequisite for DGM-CYCLE and DGM-CURL is the creation of a directed graph, which is discussed below. A directed graph is constructed from measured LAT points in 3D space. LATs are used instead of phases to enhance interpretability. They are obtained from the phases by applying a 0.8π threshold. A novel approach differing from Vandersickel et al. [2] is employed in this work to reduce parameter dependency. First, a Voronoi mesh is created from sampled points using distance r_s, forming undirected edges. Next, edges become directed based on the LAT differences between nodes through a minimum conduction velocity (CV) filter that removes edges that do not satisfy CVmin $\leq \frac{\Delta r}{\Delta \text{LAT}}$. CVmin is set to $\frac{r_s}{0.25\text{T}}$, where T is the signal period, estimated by the mean LAT difference. Finally, graphs from different time steps ($\Delta t = 0.5$T) are merged, ensuring that the edges connect over the discontinuity in the LAT field.

3.3. Directed cycle search (DGM-CYCLE)

Finding directed cycles is one of the most straightforward ways to find rotational activity in a graph. Directed cycles are found using Breadth-First-Search (BFS) on the graph previously mentioned to find the shortest directed path algorithm between every graph node and its in-neighbors. In case an in-neighbor is also an out-neighbor (ΔLAT$= 0$), the outgoing edge is temporarily removed to avoid two-cycles.

3.4. Helmholtz decomposition for directed graphs (DGM-CURL)

The Helmholtz decomposition for directed graphs, as described by Willenbourg [12], originated from land surveying to handle measurement errors in height differences. The goal is to adjust a graph's edge weights $\boldsymbol{X}$ such that the sum along any elementary cycle is zero, correcting for measurement errors. This results in two components: a curl-free graph $\boldsymbol{X}_g$ and a gradient-free graph $\boldsymbol{X}_c$, seen in Figure 1. The decomposition uses a Restricted Least Square approximation (RLSQ) with Lagrange multipliers to minimize the difference between original edge weights and these components. The cut matrix $\boldsymbol{D}$ defines the restriction. The cut matrix contains for all but one node and all edges a ± 1 or 0 if the edge is ingoing/outgoing or not adjacent to the node. The result of the cut method, using the restriction $\boldsymbol{D}\boldsymbol{X}_c = 0$ (translating to input = output for $\boldsymbol{X}_c$) is shown in Equation (2). In this paper, edge weights are set to the ΔLAT values. Rotational activity is detected from the positive components of $\boldsymbol{X}_c$, highlighting edges that contribute most to rotational activity.

$$\boldsymbol{X}_c = \left(\boldsymbol{I} - \boldsymbol{D}^T \left(\boldsymbol{D}\boldsymbol{D}^T\right)^{-1} \boldsymbol{D}\right) \boldsymbol{X} \tag{2}$$

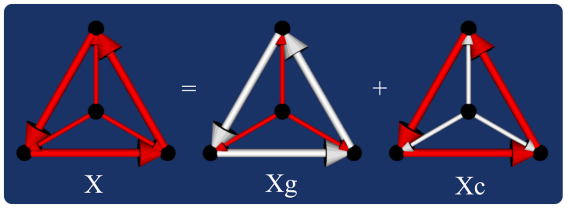

Figure 1: Illustration of the graph Helmholtz decomposition. Red edges denote non-zero edge weights, while white edges are zero.

3.5. Performance comparison

To compare the three rotor detection methods, the detections are visualized on a heat map showing the sum of the detections for each pixel divided by the duration of the signal. For phase mapping, phase singularities are used; for cycle search, cycles are reduced to their center and projected to the nearest mesh point; and for the Helmholtz decomposition, edge weights are converted to node weights by summing the outgoing edge weights. Using heatmaps avoids the parameter dependency of clustering algorithms. These heatmaps are compared to ground truth data in simulated and clinical AT datasets. The ground truth was defined as centers of rotational activity for PM, DGM-CYCLE, and DGM-CURL for the rotor simulation, and the optimal ablation line for DGM-CURL for the simulated and clinical AT data. The VF dataset lacked ground truth and was omitted. Performance was assessed using the p-value from a one-sided Mann-Whitney U test to determine whether the detected points had significantly higher weights inside the ground truth area, defined by a threshold of 5 mm. A random detector RANDOM producing random weights for each point in the graph was also included in the comparison.

4. Results and discussion

Results for the heatmaps of the detectors are shown in Figure 2 and discussed below. The rotor simulation shows that all three detectors assign large weights near the rotational center. Phase singularities have an asymmetric pattern due to the mesh structure. DGM-CYCLE detects more loops compared to PM because it considers loops of various shapes. DGM-CURL effectively identifies the rotational center but shows near-zero values due to minimization issues. Non-zero values at the mesh boundary suggest a secondary rotation. In the anatomical re-entry simulation, PM accurately detects both rotational centers, while DGM-CYCLE misses suppressed re-entries due to its reliance on directed cycles. DGM-CURL emphasizes the isthmus between the re-entries due to the "in = out" constraint of edge weights. For the clinical AT data, both PM and DGM-CYCLE detect full rotations with some skewing in DGM-CYCLE detections. DGM-CURL highlights the isthmus, indicating its stability. In the ventricle fibrillation dataset, all methods identify two main rotational centers, suggesting their role in maintaining VF. Transient rotational centers are less prominent. The Mann-Whitney U test depicted in Figure 3 confirms that all three methods effectively detect re-entries with statistically significant performance, though certain nuances in detection, like false negatives, are not captured by the p-values.

5. Conclusions

We developed DGM-CURL to detect anatomical and functional re-entry in diverse datasets. Visual analysis and low p-values ($\leq$0.0001) indicate reliable detection of rotational centers and optimal ablation targets. We recommend using multiple detection methods to improve accuracy, as each has its limitations, providing a clearer picture of cardiac arrhythmia dynamics.

References

[1] Tse G. Mechanisms of cardiac arrhythmias. Journal of Arrhythmia December 2015;32(2):75–81. ISSN 1883-2148.

[2] Vandersickel et al. Directed networks as a novel way to describe and analyze cardiac excitation: Directed graph mapping. Front Physiol 2019;.

[3] Vandersickel et al. Unique topological classification of complex reentrant atrial tachycardias enables optimal ablation strategy. Europace May 2023;25(Supplement 1). ISSN 1532-2092.

[4] Luo et al. A model of the ventricular cardiac action potential. depolarization, repolarization, and their interaction. Circulation Research 1991;68(6):1501–1526.

[5] Plank* et al. The openCARP simulation environment for cardiac electrophysiology. Computer Methods and Programs in Biomedicine 2021;208:106223.

[6] Lootens et al. Directed graph mapping exceeds phase mapping for the detection of simulated 2d meandering rotors in fibrotic tissue with added noise. Computers in Biology and Medicine March 2024;171:108138. ISSN 0010-4825.

[7] ten Tusscher et al. A model for human ventricular tissue. American Journal of Physiology Heart and Circulatory Physiology April 2004;286(4):H1573–H1589. ISSN 1522-1539.

[8] Handa BS. The effects of gap junction coupling and fibrosis on the mechanism and electrophenotype of myocardial fibrillation 2020;.

[9] Laughner et al. Processing and analysis of cardiac optical mapping data obtained with potentiometric dyes. American Journal of Physiology Heart and Circulatory Physiology October 2012;303(7):H753–H765. ISSN 1522-1539.

[10] Roney et al. Rotor tracking using phase of electrograms recorded during atrial fibrillation. Annals of Biomedical Engineering December 2016;45(4):910–923.

[11] Wieser et al. Detection of phase singularities in triangular meshes. Methods of Information in Medicine 2007; 46(06):646–654. ISSN 2511-705X.

[12] Willenborg L. Helmholtz decomposition for digraphs 2023; .

Address for correspondence:

Sebastiaan Lootens
Proeftuinstraat 86 N3, Ghent, Belgium.
sebastiaan.lootens@ugent.be

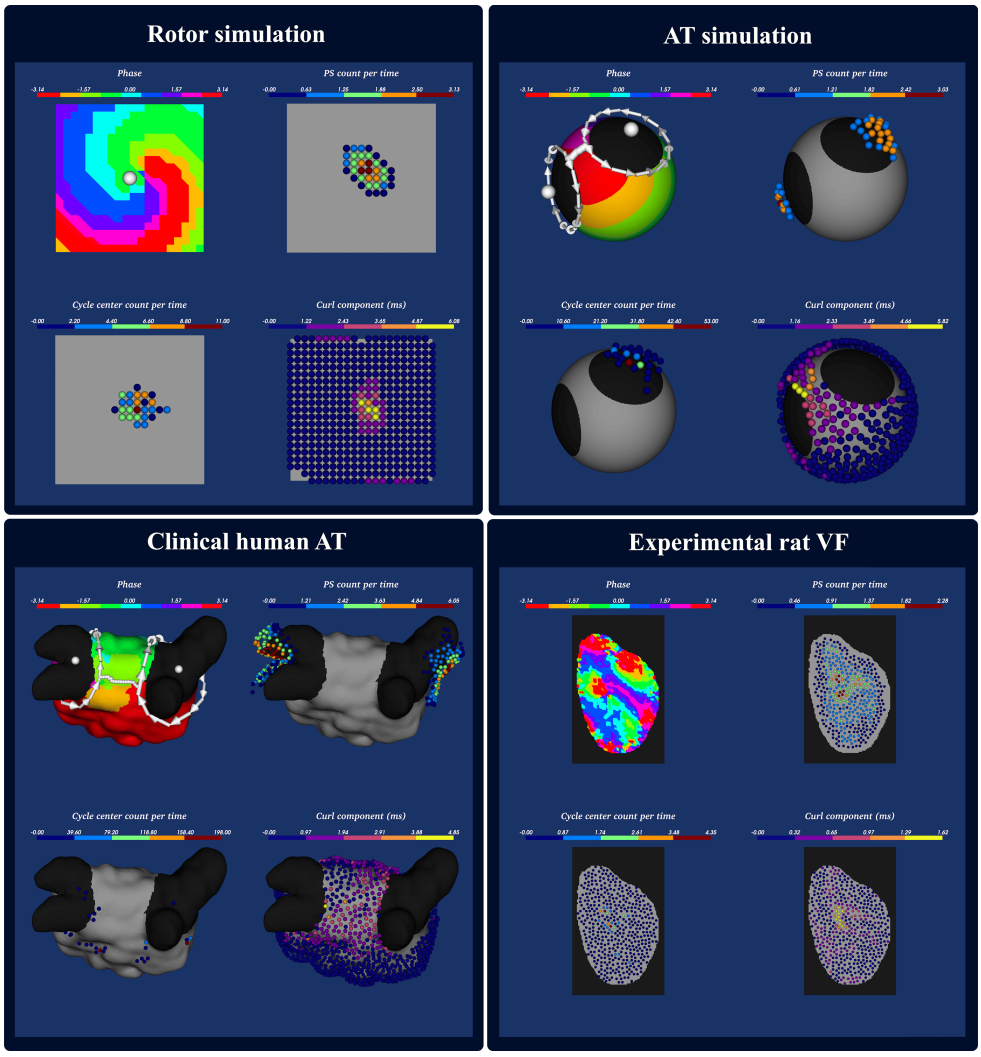

Figure 2: Heatmaps of time-averaged detection weights for PM, DGM-CYCLE and DGM-CURL along with the phase map at $t = 0$ and ground truth (white) of the analyzed data.

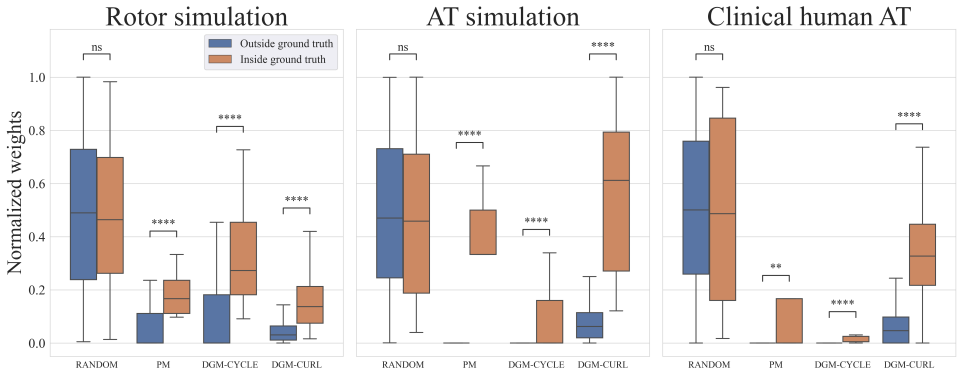

Figure 3: Mann-Whitney U test comparing time-averaged detection weights of the points inside the ground truth area ($\leq$5 mm) to the points outside the ground truth area (>5 mm) for PM, DGM-CYCLE and DGM-CURL. ns: $p > 0.05$, **: $p \leq 0.01$, ****: $p \leq 0.0001$